Journal of the European Ceramic Society **14** (1994) 143–151

Prediction of Overall Shape of Sintered Alumina Compacts

Necati Özkan & Brian J. Briscoe*

Department of Chemical Engineering and Chemical Technology, Exhibition Road, Imperial College, London SW7 2AZ, UK

(Received 19 August 1993; accepted 19 November 1993)

Abstract

The effects of the final aspect ratio on the overall shape of cylindrical sintered compacts, prepared by a uniaxial die pressing technique, are measured and described. An empirical compaction equation, which describes the compaction behaviour of a spray dried AKP-30 alumina powder, is presented. The density distribution along the axis of the compacts was predicted by using an established first-order analysis. From these predicted density distributions, the overall shapes of the sintered compacts were quite accurately predicted by using a set of sintering simulation equations obtained in separate experiments.

Der Effekt des sich ergebenden Aspektverhältnisses auf die Form von zylinderförmigen, gesinterten Preßkörpern, hergestellt durch eine einachsige Preßformtechnik, wurde bestimmt und wird im folgenden beschrieben. Eine empirische Gleichung, die das Verdichtungsverhalten von AKP-30 Aluminiumpulver beschreibt, wird angegeben. Die Dichteverteilung entlang der Probenachse wurde mit Hilfe einer etablierten Analyse erster Ordnung vorhergesagt. Ausgehend von der vorhergesagten Dichteverteilung konnten die Formen der Sinterproben, unter zuhilfenahme von Sintersimulationsgleichungen, die aus anderen Experimenten bestimmt wurden, recht gut vorhergesagt werden.

On mesure et on décrit l'influence du rapport d'aspect final sur la géométrie des cylindres frittés et compactés dans une matrice sous chargement uniaxial. On donne une équation de compactage empirique, qui permet de décrire le compactage d'une poudre d'alumine AKP-30. On a pu prédire les variations de la densité le long des cylindres par une analyse au premier ordre. Puis, à partir des distributions de densité prévues, la forme générale des cylindres frittés a pu être évaluée en utilisant un système d'équations pour la simulation du frittage obtenu par d'autres expériences.

1 Introduction

Die pressing is one of the principle preliminary consolidation techniques adopted for nominally dry ceramic precursor materials as it offers simplicity, speed, and economy of manufacture. This method is used extensively for the production of refractors, special electrical and magnetical ceramics, nuclear fuel pellets, and a variety of products for which large numbers of simple shapes are required. The die pressing technique does however have its inherent problems. The most important problem to be overcome in die pressing is the creation of a non-uniform green density. Due to the density distributions in the compacts, prepared by the die pressing technique, the shrinkage of the green may not be spatially homogeneous. As a result, the sintered compacts will not be the geometrically scaled replicas of the green compacts and their moulds, and there will be deviations from self similar geometry. The extent of these deviations will depend on the density variations in the green compact. In part, the magnitude of the deviations depends upon the size, the shape, the aspect ratio, the compaction pressure, and the compaction geometry of the compact. These factors influence the homogeneity of the stress distribution within the sample which is controlled in the major part by the wall boundary condition between the compact and the die. High wall tractions, or frictions, create greater stress gradients and hence density fluctuations. In addition, even in the absence of wall friction, for example in isostatic compaction, non-homogeneous flows occur because of the finite particle–particle frictional interactions. These interactions convey a plastic

* To whom correspondence should be addressed.

Journal of the European Ceramic Society 0955-2219/94/$7.00

character and localised flow, or shear bands, will develop. These non-uniform shear flows will also produce density variations.

The ability to control and predict the extent of the density distributions in such green compacts, and hence the overall shape of the sintered compacts, is describable in the engineering of ceramic processing operations. In this paper, the effects of the compaction pressure and the aspect ratio on the overall, fully sintered, shape of die pressed cylindrical alumina compacts are determined experimentally. By using an established first-order analysis (Janssen–Walker (J–W) analysis), the pressure variations along the pressure axis of the compacts are estimated. Various first-order compaction models, including the J–W model, have been reviewed and evaluated by Isherwood.[1] The pressure variations are then translated to the corresponding density variations by using a simple empirical equation which describes the compaction behaviour of the agglomerated powders used in this study. The density variations along the axis of the compact are then transformed to the diametrical shrinkage values by using separately established sintering equations. Hence, the amount of the final deviation from the perfect cylindrical geometry for dense bodies produced from various compacts is predicted. These predictions are then compared with the measured axial shrinkage characteristics for the same compacts.

2 Experimental procedure

A commercial alumina, designated as AKP-30 (Sumitoma—99·99% Al_2O_3) with a mean particle size of 0·4 μm, was used for the present study. The powder was dispersed in an aqueous solution of poly(vinyl alcohol) PVA (average molecular weight = 14 000, BDH Chemicals), and spray-dried to produce agglomerates for the die pressing. The agglomerated powders (typical size ~40μm), with a 2·4 wt% PVA content, were unidirectionally compacted in a 13 mm cylindrical die which was lubricated on the cylindrical die walls with zinc stearate powder (mean particle size ~3 μm, FSA Laboratory Supplies). Zinc stearate is a conventional and effective solid lubricant. No special die filling procedures were adopted. Fixed masses of the powder were poured into the die and the external walls of the die tapped to produce a relatively flat upper powder surface. Compaction was achieved using a single-ended-acting plane punch and the applied and transmitted pressures applied to the compact were measured simultaneously during compaction, using an apparatus attached to a commercial universal testing machine (Instron). A schematic outline of this apparatus is illustrated in Fig. 1. Two pressure transducers, attached to the upper and lower punches, were used to monitor the applied, Q, and the transmitted pressures, $\bar{\sigma}_{yy}$. The ratio of $\bar{\sigma}_{yy}/Q$ was designated as the transmission ratio. The signals from these transducers were amplified then transferred to an analogue–digital converter board connected to a personal computer. Three different masses of the agglomerated powder, producing a range of different aspect ratios (H/D) ($0{\cdot}52 < H/D < 1{\cdot}52$), were used to produce the non-homogeneous compacts.

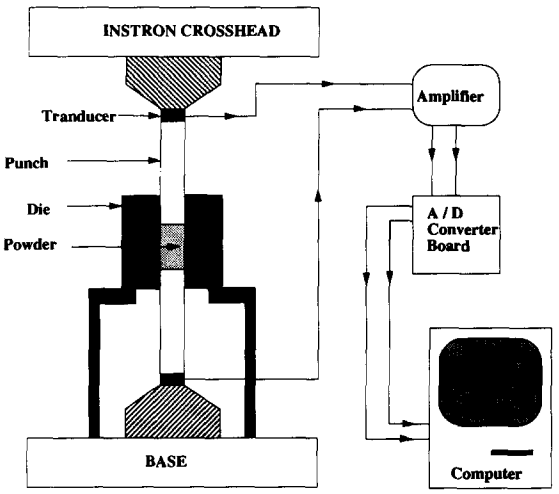

Fig. 1. The outline of the apparatus which is used to record the applied and transmitted pressures simultaneously.

In order to obtain a compaction curve (pressure–density relationship) for the agglomerated powders, relatively homogeneous compacts, with very small aspect ratios, were produced by using a range of ultimate compaction pressures. The transmission ratio of these compacts were close to unity indicating a relatively homogeneous stress distribution. These data also demonstrate that the contribution of the die wall (punch/internal cylinder) frictions to the attenuation of the stress transmission are small for these cases.

The compacts were sintered isothermally at 1527 ± 1°C for fixed times. The average sintered densities were determined using the Archimedes displacement method with distilled water as the liquid medium. Two dimensional diametric profiles of the pressed and subsequently sintered compacts were determined by using a digital micrometer with a resolution of 1 μm as a function of the cylinder height. The shapes of the surfaces adjacent to the punches were not characterised.

3 Experimental and modelling results

In order to predict the initial green density distribution and the overall sintered shape of the high

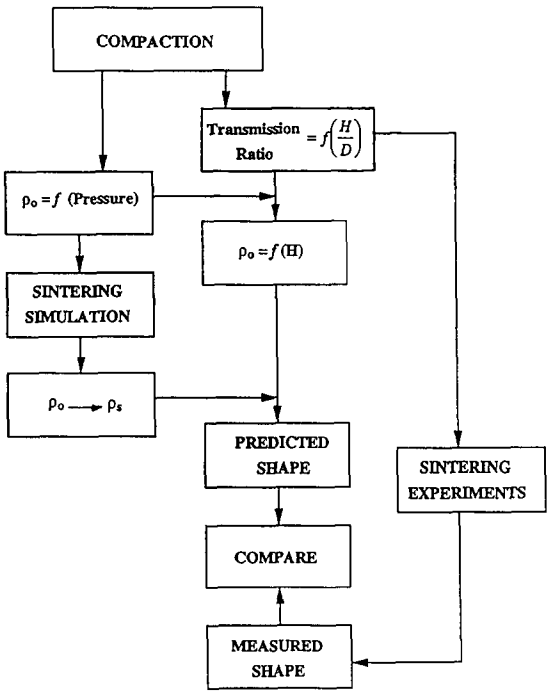

Fig. 2. The block diagram for the experimental and modelling procedure used in this study.

aspect ratio compacts, the following procedure, which is shown in Fig. 2, was applied.

(i) The transmission ratios were measured as a function of the aspect ratio.

(ii) A first-order empirical equation, which describes the interrelationship between the green density and the compaction pressure, was obtained using low aspect ratio samples.

(iii) The density distribution, as a function of the height of the compact, was then predicted using the J–W analysis by incorporating the experimental results obtained in the studies (i) and (ii) above.

(iv) Finally, the overall shape of the compact, as a function of the height of the compact, was predicted by using sintering simulation equations which interrelate the final sintered density of the compact to the predicted initial green density distribution. The results of these studies are reported in the following subsections. The next subsection, however, reports the observed shrinkage data for the samples whose behaviour is to be modelled.

3.1 The effects of aspect ratio on the transmission ratio and final sintered shape

The effects of the aspect ratio (*H/D* ratio where *H* is the terminal sample height and *D* is the die diameter) on the transmission ratio can be seen clearly by plotting the ratio of the transmitted pressure to the applied pressure (transmission ratio) against the applied pressure, an example of which is illustrated in Fig. 3. At a fixed applied pressure of 145 MPa, the overall relative densities

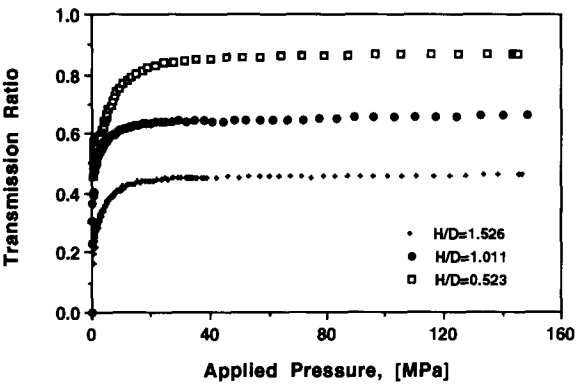

Fig. 3. The ratio of the transmitted pressure to the applied pressure versus the applied pressure for the AKP-30 alumina compacts with aspect ratios of 0·52, 1·01, and 1·53.

of the compacts with final *H/D* ratios of 0·526, 1·011, and 1·526 are 56·31%, 56·13%, and 55·84% respectively. With the increasing of the final *H/D* ratio, the influence of the friction between the powders and the die wall and between powders themselves increases, and the transmitted ratio, as a consequence, decreases. Therefore, not only will the overall density of the compacts decrease but also the density distribution will be more nonhomogeneous. The external axial shape profiles of the corresponding sintered compacts, sintered at 1527°C for 3 h, are illustrated in Fig. 4. For the final aspect ratios of 0·52, 1·01, and 1·53, the maximum gross amount of the deviation from the perfect cylindrical compact geometry, expressed as absolute diametric variations, are 27, 53, and 98 μm, respectively. The corresponding transmission ratios for the green compacts were 0·86, 0·68, and 0·47, respectively (Fig. 3).

It has been shown elsewhere[2] that low-density compacts shrink more extensively than high-density compacts. Since the transmitted pressure is always lower than the applied pressure, the compacts, produced by the die pressing, will have regions with different densities. The regions with low density will shrink more than those with high density, and as a result shape distortions in the shapes of the compacts are inevitable. With an increasing of the aspect ratio, the density variations will be greater and thus the shape distortions will be the most severe in those compacts with a high aspect ratio. This is what is observed. The following sections seek to quantify these qualitative predictions.

3.2 Compaction curves

Density–pressure, or compaction curves, have been used widely in the study of powdered materials such as metals, pharmaceuticals, and ceramics.[3,4] The compaction curves can be used to interpret the consolidation mechanism of such powders. It has been shown that when the green density is plotted as a function of the compaction

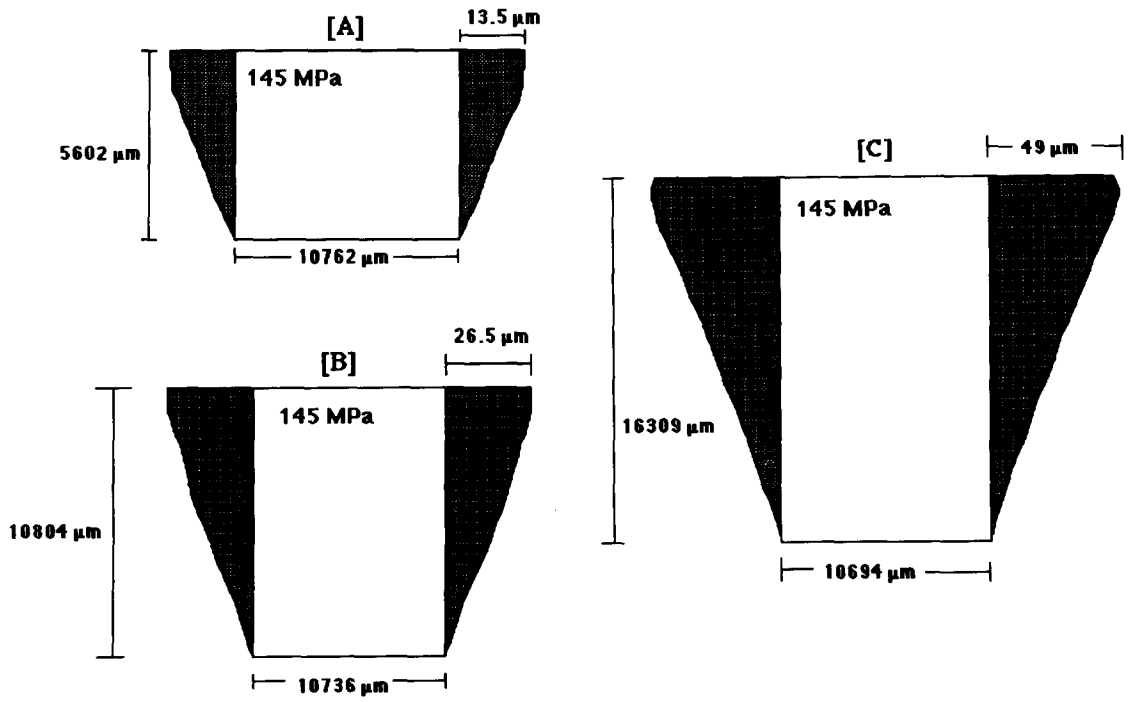

Fig. 4. The diametrical profiles of the compacts with aspect ratios of [A]. 0·52, [B] 1·01, and [C]. 1·53.

pressure for an agglomerated powder, the compaction curve shows two distinct regions. At very low pressures, very little compaction occurs until 'yield pressure' is reached at which time the agglomerates begin to deform. The compaction results for the agglomerated powders, after the yield pressure, may then be well described in the form of the following simple empirical equation:

$$\rho = A + B \log(\sigma) \qquad (1)$$

where ρ is the relative green density in % with respect to the theoretical density of the alumina (3·98 g/cm^3), σ is the compaction pressure in MPa, and A and B are parameters to be determined by experiment. In order to obtain the values of the parameters A and B, 0·75 g of the AKP-30 agglomerated alumina powders were compacted at various ultimate compaction pressures; the H/D ratios were typically ~0·15 and the corresponding transmission ratios near unity. The relative green density as a function of the compaction pressure is shown in Fig. 5. From these curves, the empirical parameters A and B for eqn (1) were obtained. This empirical compaction equation will be used for density estimations in later sections of this paper. The numerical values of A and B were estimated as 46·74 and 4·63, respectively.

3.3 Prediction of the density distribution

The compaction of a powder, constrained by a cylindrical geometry, was described by Janssen and modified by Walker.[5] The basis of the classical Janssen slice method for an element of material is illustrated in Fig. 6, the method assumes no stress (and hence in the current context density) variations in planes orthogonal to the applied stress direction.

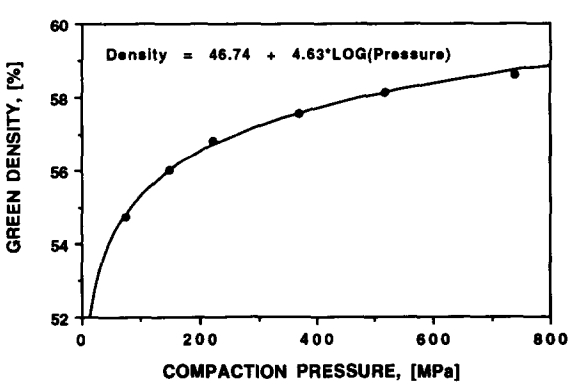

Fig. 5. The compaction curve for the AKP-30 agglomerated powder.

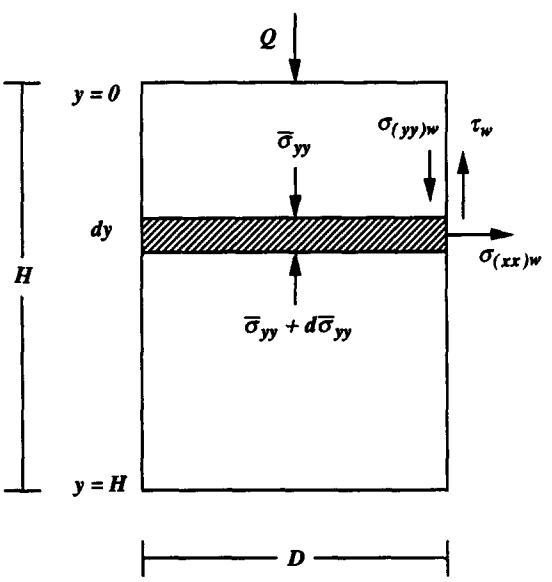

Fig. 6. Stress transmission during compaction, balance of forces.

A balance of forces on the element gives[6]

$$\frac{1}{4}\pi D^2 \, d\sigma_{yy} = -\tau_w \pi D \, dy \tag{2}$$

where D is the diameter of the cylinder, τ_w is the shear stress at the wall and σ_{yy} is the vertical stress. In the original Janssen analysis, the vertical stress was assumed to be only a function of y-direction. Walker[5] allowed for a variation of $\sigma_{(yy)}$; actually he only supposed that the wall stress $(\sigma_{yy})_w$ may differ from the vertical stress in the (mean) bulk, $\bar{\sigma}_{yy}$. These quantities were interrelated by a so called distribution factor, F, where

$$F = \frac{\sigma_{(yy)w}}{\bar{\sigma}_{yy}} \tag{3}$$

Equation (2) becomes

$$\frac{1}{4}\pi D^2 \, d\bar{\sigma}_{yy} = -\tau_w \pi D \, dy \tag{4}$$

In the original J–W treatment

$$\tau_w = \mu \sigma_{(xx)w} \tag{5}$$

where μ is the wall coefficient of friction so defined and $\sigma_{(xx)w} = K_w \sigma_{(yy)w}$ where $\sigma_{(xx)w}$ is the radial stress at the wall. The magnitude of the coefficient of K_w depends on the equilibrium state of material which is governed by the method of filling and prior history. The friction coefficient, μ, which may be function of $\sigma_{(xx)w}$, is mainly defined by the interfacial rheology of the die wall-compact interface.

Equation (4) becomes

$$\frac{1}{4}\pi D^2 \, d\bar{\sigma}_{yy} = -\mu K_w F \bar{\sigma}_{yy} \pi D \, dy \tag{6}$$

which on integration yields

$$\bar{\sigma}_{yy} = Q \exp\{-4\mu K_w F[H/D]\} \tag{7}$$

where H is the current height of the compacted cylinder and Q is the applied stress.

The ratio $\bar{\sigma}_{yy}/Q$ is the transmission ratio described previously. At $y = 0$ ($H = 0$), or at the top of the die, the mean stress is equal to the applied pressure, Q and $y = H$, or at the bottom of the die, the mean stress is equal to the transmitted pressure. In order to calculate the mean density, as a function of the height of the compact, the empirical equation, describing the experimental results, is incorporated. Equation (1) is rewritten as

$$\bar{\rho}(H) = A + B \log\{\bar{\sigma}_{yy}(H)\} \tag{8}$$

where $\bar{\rho}(H)$ is the mean density of the compact at the given height, H, of the compact and $\bar{\sigma}_{yy}(H)$ is the corresponding mean stress level. From eqns (7) and (8), we obtain:

$$\bar{\rho}(H) = A + B \log\{Q \exp(-C[H/D]\} \tag{9}$$

where $C = 4\mu K_w F$. From the slope of the plot of $\ln\{\bar{\sigma}_{yy}/Q\}$ versus $[H/D]$ (Fig. 7), C is calculated as *c.* 0·5. The computed mean density versus the height of the compact (H/D = 1·53), taking A, B, and C as 46·74, 4·63, and 0·50, respectively, is illustrated in Fig. 10(a)—see below.

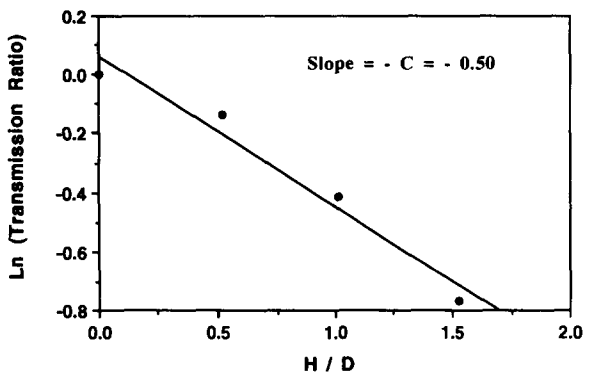

Fig. 7. The plot of $\ln(\bar{\sigma}_{yy}/Q)$ vs H/D for the AKP-30 alumina compacts.

3.4 Prediction of the overall shape of the compacts

By using sintering simulation equations, it is possible to predict, with reasonable accuracy, the shape evolution of the compacts during the sintering process. A general expression for the sintering rate can be written in the following form since the sintering rate depends on the green density and the sintered density of the compact, the diffusivity (activation energy), and the grain size:[7]

$$\frac{d\rho}{dt} = Mf(\rho) \exp(E/RT) \frac{1}{G^n} \tag{10}$$

where $M = N\Omega\gamma/RT$, N is a constant, Ω is the atomic volume, γ is the surface energy, T is the temperature, E is the activation energy, R is the gas constant, G is the grain size, n is a constant, $f(\rho)$ is the function of the green density and the sintered density. For the $f(\rho)$ parameter, the following function, adopted from Swinkels and Ashby,[8] is used.

$$\frac{1}{\left(\frac{1}{1-\rho^a}\right)\left(\left(\frac{1{\cdot}05\rho}{\rho_o}\right)^{1/b} - 1\right)\rho_o^d} \tag{11}$$

where ρ_o is the initial green density. The grain size dependence of the sintering rate is given by $1/G^n$, where n is a constant, depending upon the dominant rate controlling mechanism for the densification; $n = 3$ if the sintering is lattice diffusion controlled and $n = 4$ if it is grain boundary diffusion controlled. It has been shown that the rate controlling mechanism for the sintering in alumina is that of grain boundary diffusion.[9] During the sintering not only does densification take place, but also the grains grow in size. The driving force for

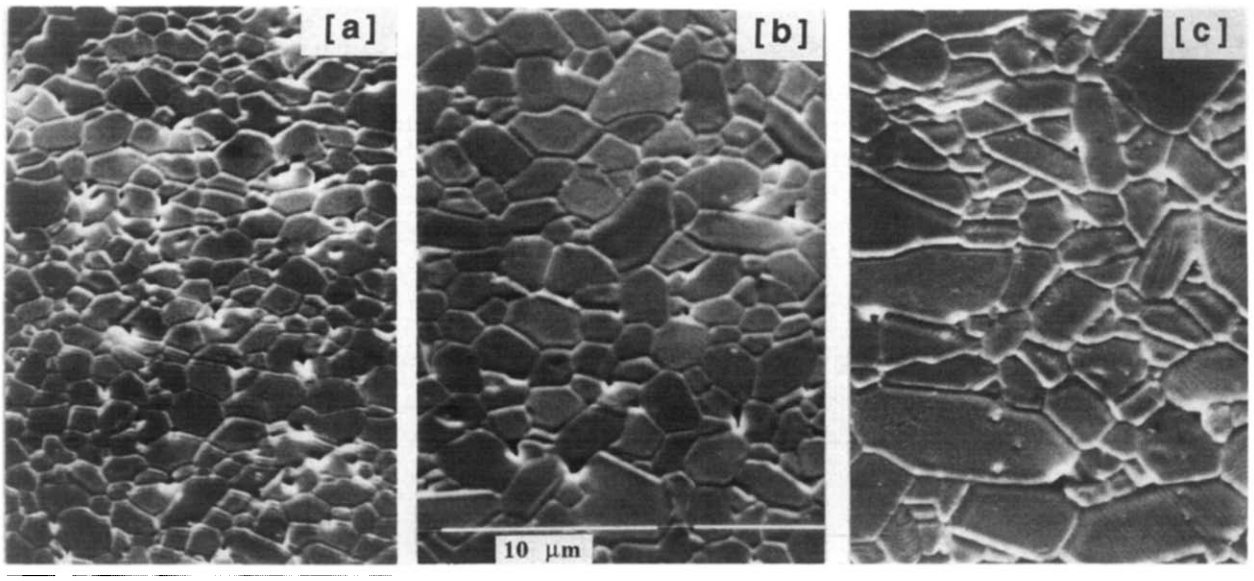

Fig. 8. The micrographs of the AKP-30 alumina compacts sintered at 1527°C for [a] 1 hour, [b] 4 hours, and [c] 11 hours.

the grain growth is the reduction in the interface energy of grain boundaries. The boundaries move toward their centre of curvature at a rate proportional to the curvature or inversely proportional to the grain diameter giving a growth law of the form:[10,11]

$$\frac{dG}{dt} = \frac{k}{G} \tag{12}$$

where k is a constant. Integrating produces

$$G^2 - G_o^2 = \frac{k}{2}t \tag{13}$$

where G_0 is the grain size at $t = 0$. However, it has been shown[12] that experiment is best represented by the following equation:

$$G^p - G_o^p = k't; \quad (p \sim 3) \tag{14}$$

In order to obtain an equation in the form of eqn (14), for the grain growth of the alumina used in this work, low aspect ratio alumina compacts were sintered at 1527°C for 30, 60, 120, 240, 420, and 660 min. The microstructure analysis was performed by using a scanning electron microscope (SEM) on polished and thermally etched surfaces of the sintered alumina compacts. The SEM micrographs of three alumina compacts are illustrated in Fig. 8. From the experimental grain growth results (Fig. 9), the parameters p and k', were estimated as 3 and $0{\cdot}78 \times 10^{-22}$ m^3/s (eqn 14).

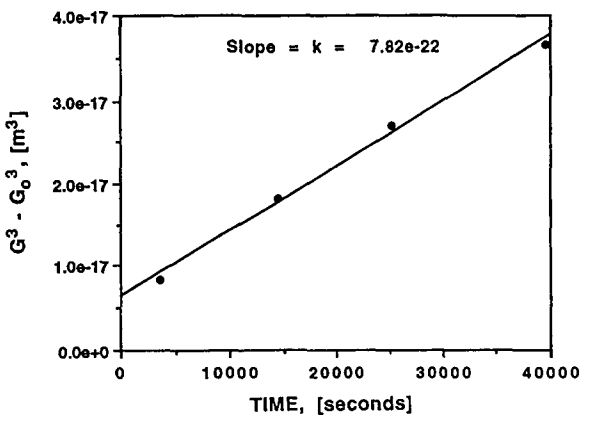

Fig. 9. G^3–G_0^3 vs time for the AKP-30 alumina compacts sintered at 1527°C.

From eqns (10) and (14) and the associated numerical values of the parameters, the density of the compact with a given initial green density was calculated at the sintering temperature as a function of the sintering time. The data used for the sintering simulation are given in Table 1.

The overall shape of the sintered compact may then be predicted by using the following equation:

$$D_s(H) = D\left\{\frac{\bar{\rho}(H)}{\bar{\rho}_s(H)}\right\}^{1/3} \tag{15}$$

where $D_s(H)$ is the diameter of the compact at the height, H, after the sintering, D is the diameter of the compact before the sintering, and $\bar{\rho}_s(H)$ is the average computed sintered density of the compact at the height, H.

This procedure implicitly assumes a non affine shrinkage in the sense that radial shrinkages in

Table 1. The data used for the sintering simulation to predict the sintered density

M (constant)	$1{\cdot}0 \times 10^{-6}$
E (activation energy)	500000 J/mol
R (gas constant)	8·3 J/mol
T (temperature)	1800 K (1527°C)
n (grain size exponent)	4
a (density function constant)	3
b (density function constant)	4
d (density function constant)	2
G_0 (initial grain size)	$0{\cdot}4 \times 10^{-6}$ m
k' (grain growth constant)	$0{\cdot}78 \times 10^{-22}$ m^3/s
p (grain growth exponent)	3

Table 2. The predicted green density, sintered density, and diameter as a function of the height of the alumina compact with H/D = 1·52

Height (mm) Green-sintered	*Green density (%) (JW-predicted)*	*Sintered density (%) (predicted)*	*'Diameter' (μm) (predicted)*
0·0–0·0	56·75	99·120	10795
2·43–2·0	56·57	99·113	10784
4·86–4·0	56·38	99·106	10772
7·29–6·0	56·19	99·098	10760
9·73–8·0	56·00	99·090	10748
12·16–10·0	55·81	99·083	10737
14·59–12·0	55·62	99·075	10724
17·02–14·0	55·43	99·068	10712
19·83–16·3	55·22	99·059	10699

each orthogonal (with respect to the compaction load axis) plane are confined only to that plane and are also autonomous; that is, each plane of shrinkage is uninfluenced by its neighbours. This assumption is of the same type as adopted, albeit in another context, in the application of the J–W analysis. The predicted compact density from J–W analysis and the corresponding sintered density, as a function of the height for a compact with a compact terminal H/D ratio of 1·52 are, given in Table 2.

It will be realised that if the green compact is sintered for a sufficiently long period then in many circumstances the sintered body will achieve a nearly spatially uniform density, say 99·0% of the theoretical density. Hence, the means for predicting the final shape may be simplified and we may obviate the need to predict the actual sintering density as described above. This route is considered further in a later section. However, the sintering simulation equations, developed to predict the sintered density of the compacts with different green densities as a function of the sintering time, are necessary to predict the shape evolution of the compacts. This facet is not considered in the present paper and will be the subject of a future publication.

3.5 Comparison of the experimental and the predicted shapes

The predicted overall shape of the compact with the H/D ratio of 1·52 is illustrated, together with the experimentally measured overall shape, in Fig. 10(b). The predicted overall shapes of the compacts with the aspect ratios of 0·52, 1·01, and 1·53, pressed at around 145 MPa are summarised in Table 3. The predicted diameters of the compacts are decreasing towards the base of the compact. It will be recalled however, the maximum diameters of the sintered compacts are slightly below the top, surcharge, end of the compact (Fig. 4). The above observations suggest that the maximum density of the compact occurs slightly below the top of the compact. There are a number of precedents for this observation provided by authors who have reported on experimental studies of the density distributions in similar types of green bodies. These authors[13–15] have reported that a low-density region appeared on the compact axis adjacent to the top punch. Since these low-density regions will shrink more than the surrounding high-density regions, therefore, the maximum diameter of the compact will not be at the top of the compact. Even though the exact features of the overall shape, near the top of the compact, are

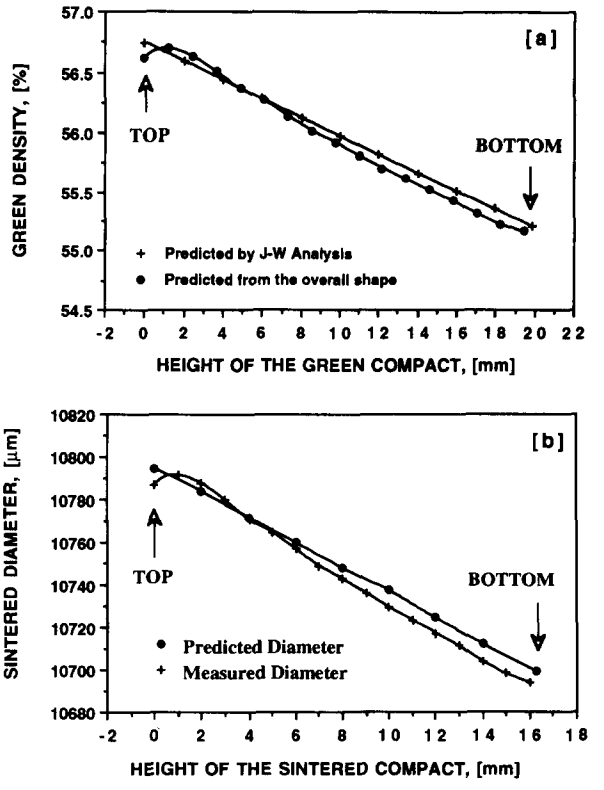

Fig. 10. [a] The green density (predicted by J–W analysis and from the overall sintered shape) as a function of the height of the green compact. [b] The predicted sintered diameter and the measured sintered diameter as a function of the height of the sintered compact.

Table 3. The overall shape of the compacts, sintered at 1527°C for 3 h

H/D	*Mean green Density (%)*	*Max. diameter (μm)*		*Min. diameter (μm)*		*Gross amount of deviation (μm)*	
		Experiment	*Predicted*	*Experiment*	*Predicted*	*Experiment*	*Predicted*
0·52	56·31	10789	10783	10762	10752	27	31
1·01	56·13	10789	10793	10736	10734	53	59
1·52	55·84	10792	10795	10694	10699	98	96

not predicted, as can be seen from Fig. 10 and Table 3, the maximum and minimum diameter of the compacts and the gross amount of deviation are predicted quite accurately. The extent of the differences between prediction and experiment is an indication of the validity of the non affine interaction assumptions incorporated within the predictive model.

The density distributions in the original compact (H/D = 1·52) may also be estimated from the overall shape of the sintered compact. The calculation of densities in greens is difficult and this procedure may provide a useful route to obtain these data. Assuming that the regions of different green density reach the same density (say 99·10%) when the sintered density of the compacts is quite near the theoretical density, the following equation, interrelating the green density of the compact to the sintered density and the sintered diameter, can be written:

$$\rho_o = \rho_s \left(\frac{D_s}{D_o}\right)^3 \tag{16}$$

where ρ_o is the green density of the compact, ρ_s is the sintered density of the compact, D_s is the diameter of the sintered compact, D_o the diameter of the green compact. The quality of these predictions will again depend upon the accuracy of the non affine assumptions incorporated into the compaction and sintering models. The density distribution, predicted from the overall shape of the sintered compact, is illustrated in Fig. 10(a) together with the density distribution which is determined by using J–W analysis combined with the associated subsidiary data. These mean radial compaction density profiles (predicted from the overall shape of the sintered compact) are consistent with experimentally determined green density profiles, for cylindrical compacts, obtained by various authors.[13–15] This agreement also vindicates the use of the procedure which includes only the initial and final densities and does not consider the evolution of shape.

4 Conclusions

The stress transmission ratio decreases as the aspect ratio of the compacts increases, and the gross amount of the deviation from the perfect cylindrical geometry for the sintered compacts is the highest for the compacts with the highest aspect ratio. Therefore, the extent of the gross deviation is closely related to the observed stress transmission ratios. That is the higher the stress transmission ratio the lower the extent of the gross deviation of the compacts. The overall shapes, but not in the detailed form, of the sintered compacts are accurately deduced from the density distributions which were determined by using J–W analysis combined with subsidiary compaction and sintering models and associated data. The primary non geometric parameter which, within the J–W analysis, controls the stress transmission is $C = 4\mu K_w F$ (eqn 9). The wall friction coefficient, μ, is the dominant term which is adjustable by the use of wall lubricants, such as zinc stearate. The friction coefficient of zinc stearate is *c.* 0·08 (Ref. 16) at high contact stresses (σ_{yy_w}).

Practically, this value of the coefficient may be regarded as the minimum which may be generally achieved in this application. Thus the levels of geometric distortion, both measured and predicted will be the lowest that probably will be encountered for the system studied. Thus, even at these modest levels of non-affine shrinkage the procedure proposed provides a good account of the shape distortions which occur during shrinkage of these compacts. In the converse sense the procedure provide reasonable mean density distributions along the height of the compacts for these systems.

Acknowledgements

The authors would like to acknowledge the financial support of British Nuclear Fuels plc for the ceramic processing programme in the Particle Technology Group at Imperial College.

References

1. Isherwood, D. P., Die wall friction effects on the compaction of polymer granules. In *Tribology in Particulate Technology*, B. J. Briscoe & M. J. Adams (eds), Adam Hilger, UK, 1987.
2. Özkan, N. & Briscoe, B. J., Effects of green density and consolidation techniques on sintering and microstructure of alumina compacts. In *Proc. Materials by Powder Technology 93*, Dresden, Germany, 1993.
3. Lukasiewicz, S. J. & Reed, J. S., Character and compaction response of spray-dried agglomerates. *Am. Cer. Soc. Bull.*, **57**(9) (1978) 798.
4. Youshaw, R. A. & Halloran, J. W., Compaction of spray-dried powders. *Am. Cer. Soc. Bull.*, **61**(2) (1982) 227.
5. Walker, D. M., An approximate theory for pressures and arching in hoppers. *Chem. Engng Sci.*, **21** (1966) 975.
6. Briscoe, B. J., Frenando, M. S. D. & Smith, A. C. The role of interface friction in the compaction of maize. In *Tribology in Particulate Technology*, eds. B. J. Briscoe & M. J. Adams. Adam Hilger, UK, 1987, p. 220.
7. Wang, J. & Raj, R. Activation energy for the sintering of two-phase alumina/zirconia ceramics. *J. Am. Cer. Soc.*, **74**(8) (1991) 1959.
8. Swinkels, F. B. & Ashby, M. F., Second report on sintering diagrams. *Acta Metall.*, **29**, (1981) 259–81.
9. Zhao, J. & Harmer, M. P., Effects of pore distribution on microstructure development: III, Model experiments. *J. Am. Cer. Soc.*, **75**(4) (1992) 830–43.

10. Kingery, W. D. & Francois, B., Grain in growth porous compacts. *J. Am. Cer. Soc.*, **48**(10) (1965) 546.
11. Nichols, F. A., Theory of grain growth in porous compacts. *J. of Appl. Phys.*, **37**(13) (1967) 4599.
12. Coble, R. L., Sintering in crystalline solids: II. *J. Appl. Phys.*, **32**(5) (1961) 793–9.
13. Train, D., An investigation into some aspects of the mechanism of pelleting. PhD thesis, Imperial College, London, UK, 1956.
14. Özkan, N., Briscoe, B. J. & Aydin, I., Density distribution in die pressed alumina compacts. In *IChemE Research Event 1994*, p. 695.
15. Macleod, H. M. & Marshall, K., The determination of density distributions in ceramic compacts using autoradiography. *Powder Technol.*, **16** (1977) 107.
16. Briscoe, B. J., Scruton, B. & Willis, F. R., The shear strength of thin lubricant films. *Proc. Royal Soc., London*, **A333** (1973) 99.